nanomaterials

MDPI

Article

Contribution of Processes in SN Electrodes to the Transport Properties of SN-N-NS Josephson Junctions

Vsevolod Ruzhickiy [1,2,3,†], Sergey Bakurskiy [1,3,†], Mikhail Kupriyanov [1,3,*], Nikolay Klenov [3,4], Igor Soloviev [1,3], Vasily Stolyarov [2,3,5] and Alexander Golubov [5,6]

1 Skobeltsyn Institute of Nuclear Physics, Lomonosov Moscow State University, 119991 Moscow, Russia
2 Dukhov All-Russia Research Institute of Automatics, 101000 Moscow, Russia
3 National University of Science and Technology MISIS, 119049 Moscow, Russia
4 Faculty of Physics, Moscow State University, 119991 Moscow, Russia
5 Center for Advanced Mesoscience and Nanotechnology, Moscow Institute of Physics and Technology, 141700 Dolgoprudny, Russia
6 Faculty of Science and Technology, MESA+ Institute for Nanotechnology, University of Twente, 7500 AE Enschede, The Netherlands
* Correspondence: mkupr@pn.sinp.msu.ru
† These authors contributed equally to this work.

Abstract: In this paper, we present a theoretical study of electronic transport in planar Josephson Superconductor–Normal Metal–Superconductor (SN-N-NS) bridges with arbitrary transparency of the SN interfaces. We formulate and solve the two-dimensional problem of finding the spatial distribution of the supercurrent in the SN electrodes. This allows us to determine the scale of the weak coupling region in the SN-N-NS bridges, i.e., to describe this structure as a serial connection between the Josephson contact and the linear inductance of the current-carrying electrodes. We show that the presence of a two-dimensional spatial current distribution in the SN electrodes leads to a modification of the current–phase relation and the critical current magnitude of the bridges. In particular, the critical current decreases as the overlap area of the SN parts of the electrodes decreases. We show that this is accompanied by a transformation of the SN-N-NS structure from an SNS-type weak link to a double-barrier SINIS contact. In addition, we find the range of interface transparency in order to optimise device performance. The features we have discovered should have a significant impact on the operation of small-scale superconducting electronic devices, and should be taken into account in their design.

Keywords: proximity effect; SNS Josephson junctions; current-phase relationship

Citation: Ruzhickiy, V.; Bakurskiy, S.; Kupriyanov, M.; Klenov, N.; Soloviev, I.; Stolyarov, V.; Golubov, A. Contribution of Processes in SN Electrodes to the Transport Properties of SN-N-NS Josephson Junctions. *Nanomaterials* **2023**, *13*, 1873. https://doi.org/10.3390/nano13121873

Academic Editor: Guy Deutscher

Received: 17 May 2023
Revised: 8 June 2023
Accepted: 13 June 2023
Published: 16 June 2023

1. Introduction

Recently, there has been renewed interest in studying planar Josephson structures with strong supercurrent concentration near the weak junction. Figure 1 shows the most common configurations of such structures. These are bridges consisting of superconducting electrodes (S) either in contact with a sublayer of normal (N) metal (Figure 1a) or simply connected by a metal bridge (Figure 1b). The structures shown in Figure 1a are called SN-N-NS bridges. The structures in Figure 1b are called variable thickness bridges (VTB) or constant thickness bridges (CTB), depending on whether the thickness of the bridge film d is equal to the thickness of the S-electrodes d_s or significantly less, respectively.

These structures are now widely used in the fabrication of nano-SQUIDs [1–11] as well as in the design and implementation of digital circuits [12–14]. The ordinary metals Nb, NbN [3–5,12,15], TiN [8,9,9], Al [2,16,17], Pb [18], Au [19–21], and Cu [22] as well as two-dimensional electron gas [23,24] and topological insulators [25–46] have been used as the weak coupling material of the Josephson elements in these devices. The calculations

performed in [47–49] indicated the prospect of using SN-N-NS bridges as basic elements of digital and analogue superconducting devices [50].

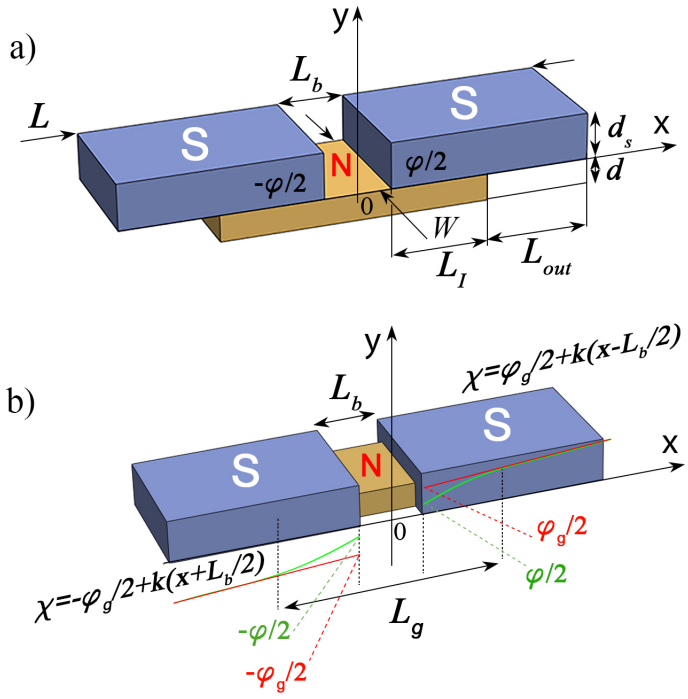

Figure 1. (**a**) Sketch of Josephson SN-N-NS bridge and (**b**) sketch of Josephson SNS bridge. Here, L_b is the distance between the S electrodes, W is the width of the structure, L_I is the length of the SN interface, d_s and d are the thickness of the S and N films, respectively, φ is the order parameter phase difference across the junctions, φ_{gl} is the global phase difference across the junction, and $\chi(x)$ is the asymptotic coordinate dependence of the electrode order parameter phase away from the weak link region.

One of the most important characteristics of the bridges is the relationship between the superconducting current I flowing through them and the phase difference φ of the order parameters of their superconducting (S) electrodes [51,52]. The question of what the value φ means and how to determine it correctly depends both on the geometry of the Josephson structure and on the transport properties of its boundaries.

In this paper, we solve this question regarding SN-N-NS Josephson bridges. It is important to note that the developed approach can be applied to any structure in which there is a concentration of supercurrentin S-electrodes in the vicinity of their boundary with the weak coupling region.

2. Correct Determination of φ as Measured by Experiment

The problem of correctly defining φ has been conventionally solved in the simplest model, the so-called Rigid Boundary Conditions (RBC), to describe the properties of the S-electrodes. The RBC model has been the workhorse model most often used in the analysis of processes in Josephson junctions [53–58]. It is assumed that all nonlinear and non-equilibrium processes in Josephson structures are localized in the weak coupling region between two two superconducting (S) electrodes (see Figure 1b). Reverse effects of these processes on electrode superconductivity are considered to be negligible. The electrodes are in a stationary and equilibrium state, so that the order parameter modules Δ_0 and the anomalous Green functions characterizing their superconducting state are independent of the spatial coordinates and coincide with their equilibrium values calculated for a solitary superconductor. In this model, the setting of a bias current through the Josephson contact is provided by a χ linearly increasing with the coordinate phase of the order parameter

$\Delta = \Delta_0 \exp\{i\chi\}$, which experiences a jump at the geometric boundary of the weak coupling region by the value φ (the red line in Figure 1b). This value is often called the Josephson phase difference at contact [51].

Further research allowed us to formulate the areas of applicability of this model for the case of almost equal thickness and width of the N and S films. It has been demonstrated [59–66] that suppression of superconductivity in S electrodes due to the proximity effect and the effect of depairing of superconducting correlations by bias supercurrent leads to a mismatch between the phases of Green's function and the order parameter at the NS boundaries, which no longer coincide with each other. For this reason, it is impossible to introduce a physically meaningful Josephson phase difference φ between the NS interfaces.

The suppression of superconducting correlations in the vicinity of the interfaces of S electrodes with the material of the weak coupling region actually means the spatial expansion of this region. It is no longer determined by the geometric boundaries separating the materials of the structure, so that the Josephson phase difference of the order parameters φ becomes not a measurable quantity and in no way characterizes the properties of the Josephson structure. The weak coupling region expands up to the values of L_g. This length defines the positions of the regions inside the S electrodes, outside of which the modules of both Δ_0 and the anomalous Green's functions reach values independent of spatial coordinates and their phases coincide with each other and increase linearly with the growth of the coordinate x along the x-axis. Extrapolation of this linear dependence to the geometric boundaries of materials determines the global Josephson phase difference φ_g. The introduction of φ_g allows us to consider the Josephson contact as a serial connection of the structure with the current–phase relation $I(\varphi_g)$ and the inductance of the S electrodes. All effects initiated by delocalization of the weak link region (the green line in Figure 1) are taken into account in the shape of the $I(\varphi_g)$ dependence. This provides a junction description convenient for designing and studying processes in devices having such delocalised Josephson contacts.

In [67], it was concluded that the desired parameters of the Josephson contact $I_c \sim 0.1$ mA, $I_c R_N \sim 0.8$ mV can be achieved at $L_b \sim 50$ nm, $W \sim 40$ nm. These scales are quite comfortable for modern methods in the CMOS industry. The problem is to obtain such I_c and $I_c R_N$ with accuracy 2%, and these lengths should be implemented with an accuracy up to 1 nm. Because implementation of this accuracy in the bridge-type planar technologies used for superconducting VLSI circuits would require very advanced CMOS nodes, the authors of [67] concluded that this type of junction can be used only in devices in which the parameter spreads are not important.

In fact, such a rigorous conclusion is rather a consequence of the specific geometry of bridge shown in Figure 1b. Recently [47], it was demonstrated that in the bridge geometry shown in Figure 1a there are no such strict restrictions on W, L_b, and d. This is due to the delocalization of the weak region due to the finite transparency of the SN boundaries.

In the microscopic theory of superconductivity [68,69], the presence of a finite transparency of the interface between a massive superconductor and a thin non-superconducting metal is characterized by a suppression parameter $\gamma_{BM} = \gamma_B d/\xi_n$, $\gamma_B = (R\xi_s)/(\rho_n \xi_n)$. Here, R is the specific boundary resistance, ξ_s is the coherence length of the S electrodes, and ρ_n and ξ_n are the resistivity and decay length, respectively, of the weak link material. Typical values of the suppression parameter $\gamma_{BM} = 1 \div 3$ at interfaces between Nb and a thin Al film were obtained by comparing theoretical predictions [69] with experimental results [70–72] obtained in NbAl-AlO_x-Nb and NbAl-AlO_x-AlNb tunnel structures. The existence of a finite interface transparency between two normal metals was confirmed experimentally in [73–78].

In an SN-N-NS bridge, the finite interface transparency leads to violation of the rigid boundary conditions used in the above estimates [67] and delocalization of the weak coupling region [47] (see Figure 1a). In the limit $L_b \lesssim \xi_n$, both the critical current I_c and the $I_c R_N$ product are mainly determined in these junctions by the suppression parameter γ_{BM} rather than by the bridge geometrical factors L_b and W. There is no need for additional

structuring of the width of the bridge film [47]. Its width may coincide with the width of the composite electrode, and may be determined by the requirements for the line width of a technological process. In MIT Lincoln Laboratory technology, the lower and upper limits on W (150 nm $\lesssim W \lesssim$ 250 nm) are determined by the requirement of current carrying capacity and uniformity of the bias current distribution across the width of the electrodes, respectively [79]. There are no strict requirements for the reproducibility of the gap between the electrodes formulated in [67]. Due to the delocalization of processes in the weak link region, its effective size along the direction of the current significantly exceeds L_b. Moreover, numerical calculations show that in SN-N-NS junctions at $L_b \lesssim \xi$ and $\gamma_{BM} \gtrsim 1$, the critical current is practically independent on L_b.

However, it should be noted that the conclusions formulated in [47] were obtained under the assumption that the phase of the electrode order parameter at the SN boundaries $\chi(x,0) = \pm\varphi/2 = const$ does not depend on the coordinate x. Obviously, this assumption is too strong. It does not take into account the heterogeneous nature of the current supply from the N-film to the S-electrode, and leads to a violation of the current conservation law ($divJ = 0$) in composite SN-electrodes. Thus, even in the absence of superconductivity suppression in the S part of a composite SN electrode, $\chi(x,0)$ should depend on x due to the mutual nature of the proximity effect and the effect of current suppression of superconductivity, and cannot be used as an argument in the current-phase relation. The solution to this problem is to formulate and solve the two-dimensional problem of finding the spatial distribution of the supercurrent in the SN electrodes, determining φ_g, and finding the $I(\varphi_g)$ relation. This is exactly the purpose of the present work.

3. Model

We consider a normal (N) metal film connecting two massive superconducting (S) electrodes of length $L_I + L_{out}$ located at a distance $\pm L/2$ from the center of the film (see Figure 1a). Here, L_I is the length of overlap between the S and N layers, while L_{out} is the length of the free outer part of the S electrode. We place the origin of coordinates on the upper surface of the N film in the middle of the SN-N-NS structure and direct the x and y axes along and perpendicular to the SN interfaces, respectively. The existence of the proximity effect between the N and S materials should lead to the induction of superconducting correlations into the N metal, leading to Josephson coupling between the S banks.

We suppose that the dirty limit condition is satisfied for all the metals, the critical temperature of the weak link material is equal to zero, and its thickness d is much smaller than the decay length $\xi_n = (D/2\pi T_c)^{1/2}$. Here, D, is the diffusion coefficient of the weak link material and T_c is the critical temperature of the S electrode. In the normal metals commonly used in technology, such as Cu, Au, and Al, the coherence length is ξ_n 50–100 nm (see [78,80] and references therein). Thus, for N layers with a thickness of d 5–10 nm, it is easy to realize a strong inequality between d and ξ_n. Due to the symmetry of the problem, we may consider it for positive x only.

The conditions

$$d \ll \xi_n,\ \gamma_m = \frac{\rho_n \xi_n}{\rho_s \xi_s} \frac{d}{\xi_n} \ll 1 \tag{1}$$

permit us to neglect the suppression of superconductivity in the S film due to proximity effect and reduce the two-dimensional Usadel equations [81] in the N film to a one-dimensional problem [47,49]:

$$\xi_{eff}^2 \frac{\partial}{\partial x}\left(G^2 \frac{\partial \Phi}{\partial x}\right) - \Phi = -\delta \exp\{i\chi(x,0)\}, \tag{2}$$

$$L_b/2 \le x \le (L_I + L_b)/2$$

$$\xi_{eff}^2 = \frac{\gamma_{BM}}{G(G_s + \gamma_{BM}\omega)},\ \delta = \frac{G_s\Delta}{(G_s + \gamma_{BM}\omega)}. \tag{3}$$

$$\frac{\partial}{\partial x}\left(G^2\frac{\partial\Phi}{\partial x}\right) - \omega G\Phi = 0,\ 0 \le x \le L_b/2 \tag{4}$$

Here, Φ and $G = \omega/(\omega^2 + \Phi\Phi^*)^{-1/2}$ are Usadel Green's functions, $\omega = (2n+1)T/T_C$ are Matsubara frequencies normalized on πT_C, the coordinate x is normalized on ξ_n, the modulus of the order parameter in the S electrode Δ is normalized on πT_C, and ρ_s and ξ_s are the resistivity and coherence length of the S film, respectively.

Due to (1), we assume that the suppression of superconductivity in the S electrodes is negligible and that the value of the critical junction current I_c is significantly less than the preparation current of the S films. Under these conditions from the Usadel equation in the S electrodes, it follows that in this approximation the phases of the order parameter $\Delta(x,y)$ and anomalous Usadel Green's functions $\Phi_s(x,y)$ coincide with each other, while their modules equal their equilibrium values in a superconductor at a given temperature T:

$$\Phi_s(x,y) = \Delta(x,y) = \Delta_0\exp\{\chi(x,y)\},\ G_s = \frac{\omega}{\sqrt{\omega^2 + \Delta_0^2}}. \tag{5}$$

The phase $\chi(x,y)$ obeys the Laplace equation

$$\frac{\partial^2}{\partial x^2}\chi + \frac{\partial^2}{\partial y^2}\chi = 0. \tag{6}$$

It is convenient to normalize the x and y coordinates in (6) as well as all of the geometrical lengths d_n, d_s, L_b, L_I, L_{out} on ξ_n. Equations (2), (4) and (6) must be supplemented by the boundary conditions.

At $x = L_b/2$, they are determined from the requirement of continuity of the Φ functions and their first derivatives:

$$\frac{\partial\Phi(L_b/2+0)}{\partial x} = \frac{\partial\Phi(L_b/2-0)}{\partial x}, \tag{7}$$

$$\Phi(\frac{L_b}{2}+0) = \Phi(\frac{L_b}{2}-0).$$

At $x = L_b/2 + L_I$,

$$\frac{\partial}{\partial x}\Phi = 0, \tag{8}$$

and at $x = 0$,

$$\frac{\partial}{\partial x}\mathrm{Re}\Phi = 0,\ \mathrm{Im}\Phi = 0 \tag{9}$$

where $\mathrm{Re}\Phi$ and $\mathrm{Im}\Phi$ are the real and imaginary parts of Φ, respectively.

At $x = L_b/2$, $0 \le y \le d_s$, $y = d_s$, $L_b/2 \le x \le L/2$, and $y = 0$, $L_b/2 + L_I \le x \le L/2$, which follow from the demand of absence of any supercurrent across the interfaces

$$\frac{\partial}{\partial x}\chi(\frac{L_b}{2}, y) = 0,\ \frac{\partial}{\partial y}\chi(x, d_s) = 0,\ \frac{\partial}{\partial y}\chi(x,0) = 0. \tag{10}$$

We further assume that the characteristic size of the S electrodes $(L - L_b)/2$ significantly exceeds the characteristic lengths (ξ_n, ξ_{eff}) at which a spatial redistribution of the supercurrent density $\mathbf{J}_s$

$$\mathbf{J}_s(x,y) = \{J_{sx}, J_{sy}\} = S_1\nabla\chi(x,y), \tag{11}$$

$$S_1 = \frac{2\pi T}{e\rho_s\xi_n}\sum_{\omega>0}^{\infty}\frac{G_s^2\Delta_0^2}{\omega^2}$$

in the S electrodes is possible. Under this condition, at $x = L/2$, $0 \le y \le d_s$ there is a uniform distribution of the superconducting current density $\mathbf{J}_s$ over the thickness of the S and N films, that is, $J_y = 0$ and

$$J_{sx} = S_1\frac{d}{dx}\chi(L_g/2, y) = \frac{I}{d_s}, \tag{12}$$

where I is a full supercurrent flow across the junction. Expression (12) determines the boundary condition at $x = L/2$.

$$\frac{d}{dx}\chi(L/2, y) = \frac{I}{S_1 d_s},\ 0 \le y \le d_s. \tag{13}$$

The last boundary condition at $y = 0$, $L_b/2 \le x \le L_b/2 + L_I/2$ follows from the current conservation low as well. It reads that decay of supercurrent I_n in the weak link film at a point x located under the S electrode should be equal to the density of supercurrent injected at this point into this S electrode:

$$S_1\frac{d}{dy}\chi(x, 0) = \frac{d}{dx}I_n, \tag{14}$$

$$\frac{I_n(x)}{I_0} = \frac{T}{T_c}\sum_{\omega\ge0}^{\infty}\frac{G^2}{\omega^2}\left(\mathrm{Im}\Phi\frac{\partial \mathrm{Re}\Phi}{\partial x} - \mathrm{Re}\Phi\frac{\partial \mathrm{Im}\Phi}{\partial x}\right), \tag{15}$$

where $I_0 = J_0 W d$, $J_0 = 2\pi T_c/e\xi_n\rho_n$, and W is the width of the structure.

The boundary value problem formulated above was solved by numerical methods. It is naturally divided into two interrelated tasks. The first consists of calculating the distribution of the supercurrent (15) along the normal film, that is, in solving the boundary value problem (2), (4), (7)–(10) for a given phase distribution $\chi(x, 0)$. The second task is to use the finite element method to find the dependencies of $\chi(x, y)$ and $\mathbf{J}_s(x, y)$ by solving the Laplace Equation (6) with the boundary conditions (10), (13), (14). The solution of the Laplace equation $\chi(x, y)$ is determined up to a constant. We chose its value from the condition $\chi(L_b/2, 0) = \varphi/2$.

Calculation of current characteristics can be accomplished using the iterative method for a given phase φ. At the zeroth iteration, a calculation is made for a constant value of the superconducting phase $\chi(x, 0) = \varphi/2 = const$ along the S electrode. The obtained value of the total current I and the derivative of the current dI_n/dx along the electrode are used as the boundary conditions for solving the problem for the S electrode. In the next step, we substitute the resulting distribution $\chi(x, 0)$ into the Usadel's Equations (2) and (4). Then, the iterative cycle is repeated until the value of the critical current stops changing. With the values of the parameters under consideration, four iterative cycles are sufficient for this. Extrapolation of the linear dependence $\chi(x, 0)$ obtained in the region $x \approx L/2$ on the boundary of the composite SN electrode with bridge film $(x = L_b/2)$ determines φ_g, and allows us to find the desired dependence $I(\varphi_g)$.

In the practical implementation of the calculation method described above, we limited ourselves to the following set of parameters: $T/T_c = 0.5$, $\varphi = \pi/2$, $d_n/\xi_n = 0.1$, $d_s/\xi_n = 10$, $L_{out} = 10$, $\rho_s/\rho_n = 10$, $L_b/\xi_n = 0.1$. We performed the calculation for two values: $\gamma_{BM} = 1, 0.5$ and $L_I/\xi_n = 20, 4, 0.5$. The calculation results are shown in Figures 2–5.

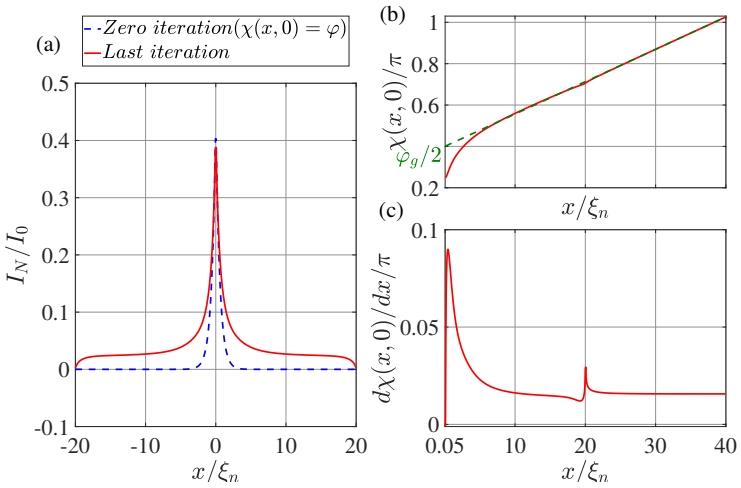

Figure 2. (**a**) The coordinate dependence of the current I_n flowing through the N film. The dotted blue line shows the result obtained at the zeroth iteration ($\chi(x,0)=\varphi$), while the solid red line shows the dependence obtained at the last iteration. (**b**) Distribution of phase of the superconducting order parameter $\chi(x,0)$ at the last iteration. The dotted green line shows the linear extrapolation of the $\chi(x,0)$ function from the region $x \leq L/2$. (**c**) The derivative of the phase of the order parameter as a function of coordinate x at the last iteration. Calculations have been performed for $T/T_c = 0.5$, $L_I/\xi_n = 20$, $\varphi = \pi/2$, $d_n/\xi_n = 0.1$, $d_s/\xi_n = 10$, $L = 80$, $\rho_s/\rho_n = 10$, $\gamma_{BM} = 0.5$, $L_b/\xi_n = 0.1$.

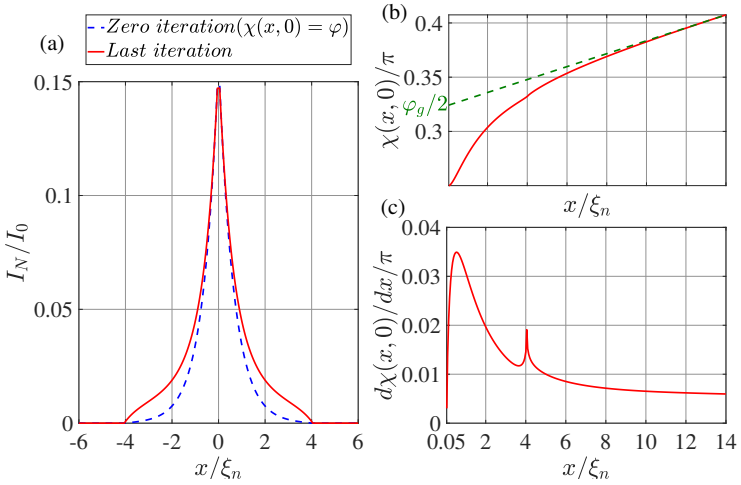

Figure 3. (**a**) The coordinate dependence of the current I_n flowing through the N film. The dotted blue line shows the result obtained at the zeroth iteration ($\chi(x,0)=\varphi$), while the solid red line shows the dependence obtained at the last iteration. (**b**) Distribution of phase of the superconducting order parameter $\chi(x,0)$ at the last iteration. The dotted green line shows the linear extrapolation of the function $\chi(x,0)$ from the region $x \leq L/2$. (**c**) The derivative of the phase of the order parameter as a function of coordinate x at the last iteration. Calculations have been performed for $T/T_c = 0.5$, $L_I/\xi_n = 4$, $\varphi = \pi/2$, $d_n/\xi_n = 0.1$, $d_s/\xi_n = 10$, $L = 28$, $\rho_s/\rho_n = 10$, $\gamma_{BM} = 1$, $L_b/\xi_n = 0.1$.

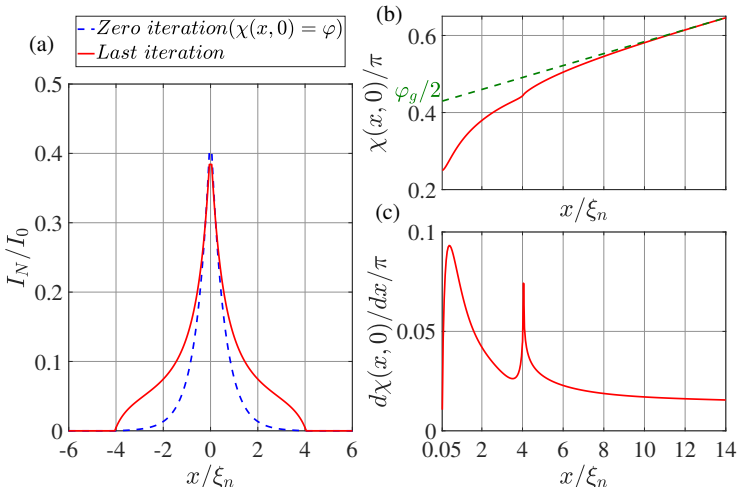

Figure 4. (**a**) The coordinate dependence of the current I_n flowing through the N film. The dotted blue line shows the result obtained at the zeroth iteration ($\chi(x,0)=\varphi$), while the solid red line shows the dependence obtained at the last iteration. (**b**) Distribution of phase of the superconducting order parameter $\chi(x,0)$ at the last iteration. The dotted green line shows the linear extrapolation of the function $\chi(x,0)$ from the region $x \leq L/2$. (**c**) The derivative of the phase of the order parameter as a function of coordinate x at the last iteration. Calculations have been performed for $T/T_c = 0.5$, $L_I/\xi_n = 4$, $\varphi = \pi/2$, $d_n/\xi_n = 0.1$, $d_s/\xi_n = 10$, $L = 28$, $\rho_s/\rho_n = 10$, $\gamma_{BM} = 0.5$, $L_b/\xi_n = 0.1$.

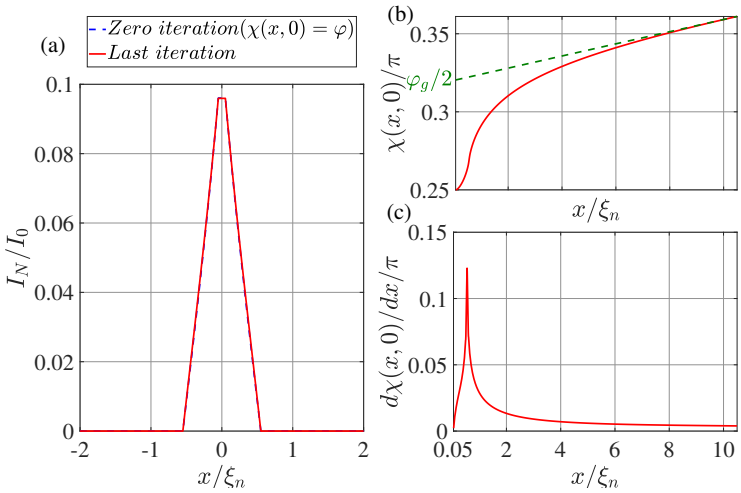

Figure 5. (**a**) The coordinate dependence of the current I_n flowing through the N film. The dotted blue line shows the result obtained at the zeroth iteration ($\chi(x,0)=\varphi$), while the solid red line shows the dependence obtained at the last iteration. (**b**) Distribution of phase of the superconducting order parameter $\chi(x,0)$ at the last iteration. The dotted green line shows the linear extrapolation of the function $\chi(x,0)$ from the region $x \leq L/2$. (**c**) The derivative of the phase of the order parameter as a function of coordinate x at the last iteration. Calculations have been performed for $T/T_c = 0.5$, $L_I/\xi_n = 0.5$, $\varphi = \pi/2$, $d_n/\xi_n = 0.1$, $d_s/\xi_n = 10$, $L = 20$, $\rho_s/\rho_n = 10$, $\gamma_{BM} = 1$, $L_b/\xi_n = 0.1$.

4. Supercurrent Distribution in the N Part of SN Electrodes

The dotted blue line in Figures 2a–5a shows the supercurrent distribution in the N part of SN electrodes at the initial step of iteration. It can be seen that at $L_I/\xi_n = 20$ (see Figure 2a) in this step the current completely outflows from the N layer into the S film at a characteristic length of ξ_{eff}. Note that it is this current distribution that was used earlier in [47] when calculating the parameters of SN-N-NS bridges. The iterative solution of the problem presented in Figure 2a by the solid red line shows that the area in which the currents are redistributed between the N and S films is expanding. Moreover, part I_n of the full current continues to flow along the N layer even away from the bridge, reaching

a value that is weakly dependent on x. There is practically no leakage of current from the N to the S part of the SN electrode in this area. This component of the current finally leaves the N layer in the vicinity of $x = L_I/2$. The area in which I_n weakly depends on x shrinks with decreasing L_I. Thus, with $L_I/\xi_n = 4$ (see Figures 3a and 4a), the difference in the dependencies of $I_n(x)$ at the initial (solid blue line) and final (dotted red line) iteration stages is no longer so significant. The smaller it is, the larger the parameter γ_{BM}, that is, the larger ξ_{eff}. Finally, for $L_I < \xi_{eff}$, the current component I_n turns out to be independent of x. In this case, the current is injected into the S film through a small area without changing the phase of the order parameter along the SN boundary, meaning that $\chi(x,0) = \varphi$. This is confirmed by the numerical calculations for $L_I/\xi_n = 0.5$ presented in Figure 5a.

5. Spatial Dependence of the Order Parameter Phase $\chi(x,0)$ along the SN Interface

It is convenient to analyze the nature of current leakage from the N film into the S electrode by examining the coordinate dependencies of the phase of the superconductor order parameter along the SN boundary shown in Figures 2b,c–5b,c. It can be seen that regardless of the values of L_I in the vicinity of $x = L_b/2$ there is a sharp increase in the derivatives $d\chi(x,0)/dx$ to values several times larger than their values in the region of $x \lesssim L_I$. After reaching the maximum, the derivatives decrease, experiencing a singularity at $x = L_b/2 + L_I$ due to the final leakage of current into the S electrode.

This behavior of $\chi(x,0)$ indicates a significant concentration of J_{sx} components of the current density in the vicinity of $x \gtrsim L_b/2$.

Figures 6 and 7 show spatial distributions of $J_x(x,y)$ and $J_y(x,y)$ supercurrent components in the SN-N-NS bridge calculated for $L_I/\xi_n = 4$ and $\varphi = \pi/2$. These spatial distributions clearly demonstrate that in the region $L_b/2 \lesssim x \lesssim L_b/2 + L_{jx}$ with $L_{jx} \approx 1.5\xi_n$, the concentration of the current component J_x really occurs in an area whose thickness is about 4 times less than d_s. The characteristic scale L_{jy} of the injection area of the current component J_y into the S electrode is approximately equal to $0.6\xi_n$. With $\gamma_{BM} = 0.5$, this is completely consistent with the theoretical estimate of the size of this region $\xi_n(\gamma_{BM})^{1/2}$ in [47].

It should be noted that the difference between L_{jx} and L_{jy} is due to the fact that L_{jy} is determined by the value ξ_{eff} at $\omega = \pi T$, while L_{jx} plays the role of the Josephson penetration depth and is inversely proportional to the square root of the local value of critical current density of the SN interface.

The concentration of the current component J_x leads to an increase in the local inductance value L_{loc} per unit length of this region, which is inversely proportional to the characteristic scale of the current concentration region. This scale turns out to be significantly less than d_s. To extract the additional contribution in L_{loc} from the magnitude of the linear inductance of the S-electrode L_{lin}, we must determine the magnitude of φ_g:

$$\frac{\varphi_g}{2} = \chi\left(\frac{L}{2}, 0\right) - \frac{d\chi(L/2,0)}{dx}\left(\frac{(L-L_b)}{2}\right) \tag{16}$$

as shown in Figures 2b–5b. The dotted line in Figures 2b–5b shows the asymptotic dependence of $\chi(x,0)$ for large values of x, which determines the value of $\varphi_g/2$ for $x = L_b/2$. This definition of φ_g opens up the possibility of representing the SN-N-NS structure in the form of two bundled elements connected in series, namely, the Josephson junction with CPR $I(\varphi_g)$ and the linear inductance L_{lin} of the S film.

Such an equivalent scheme of Josephson contact actually implies taking into account part of the inductance of the S electrodes in the form of changing the shape of contact current–phase relation. With this description, the part of the S electrodes ($L_b/2 \le x \le L_{gl}/2$) in which there is a noticeable deviation of the dependence of $\chi(x,0)$ from the linear one formally turns out to belong to the weak coupling region. The calculation results presented in Figures 2b–5b allow us to conclude that $L_{gl} \approx 5\xi_n$ and weakly depend on L_I and γ_{BM}.

It is interesting to note that a completely opposite procedure was proposed earlier in the RBC model [82]. In [82], the authors suggested describing a Josephson contact with

non-sinusoidal dependence $I(\varphi)$ as a series connection of inductance and contact with a sinusoidal of the $I(\varphi)$ relation.

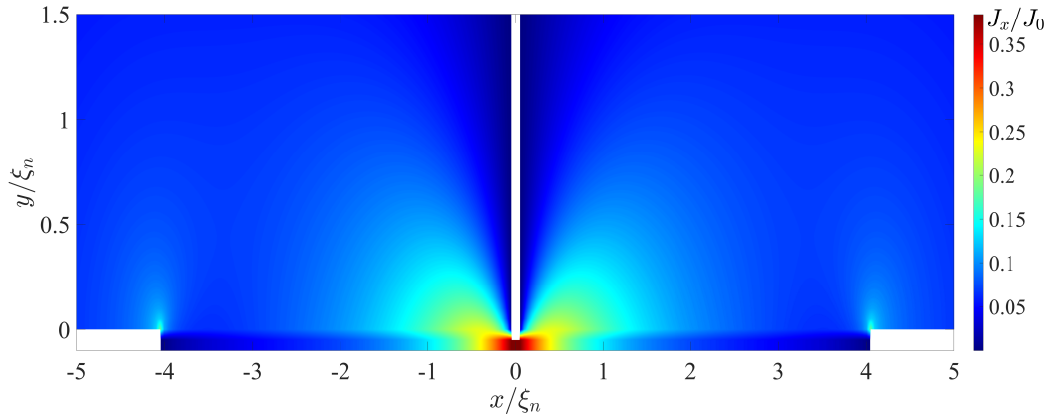

Figure 6. Coordinate dependence of the $J_x(x, y)$ component of the supercurrent density calculated for $T/T_c = 0.5$, $L_I/\xi_n = 4$, $\varphi = \pi/2$, $d_n/\xi_n = 0.1$, $d_s/\xi_n = 10$, $L = 28$, $\rho_s/\rho_n = 10$, $\gamma_{BM} = 0.5$, $L_b/\xi_n = 0.1$.

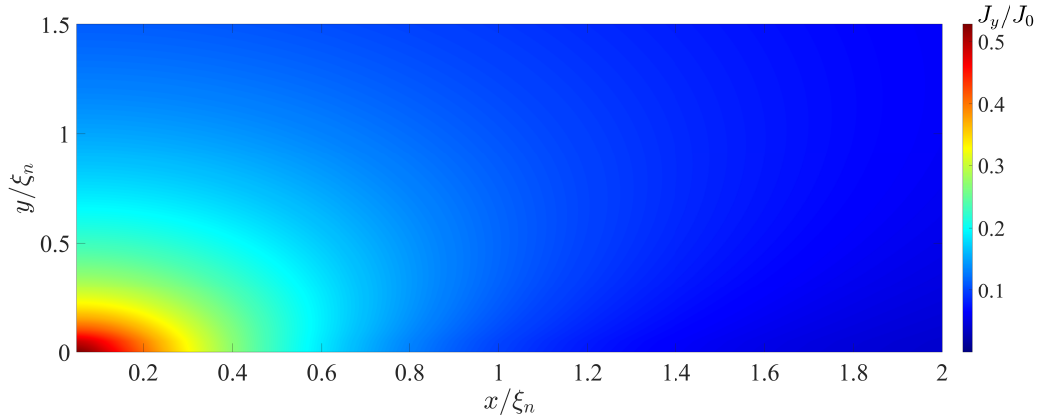

Figure 7. Coordinate dependence of the $J_y(x, y)$ component of the supercurrent density calculated for $T/T_c = 0.5$, $L_I/\xi_n = 4$, $\varphi = \pi/2$, $d_n/\xi_n = 0.1$, $d_s/\xi_n = 10$, $L = 28$, $\rho_s/\rho_n = 10$, $\gamma_{BM} = 0.5$, $L_b/\xi_n = 0.1$.

6. Current–Phase Relation $I_s(\varphi_{gI})$

Our numerical calculations show that the shape of the current–phase relation $I(\varphi)$ for $T/T_c = 0.5$ and $L_I/\xi_n \gtrsim 2$ (see Figure 8) differs slightly from the one calculated earlier in [47]. It is close to a sinusoidal shape; however, unlike the results obtained in [47], the maximum in $I(\varphi)$ is slightly shifted not to the area of $\varphi > \pi/2$, but towards $\varphi < \pi/2$. Such deformation is typical for Josephson structures, as the superconductivity of their electrodes is suppressed by the current flowing through them [59,61,63]. This indicates that in SN-N-NS bridges in the region $L_b/2 \leq x \lesssim L_b/2 + \xi_n$ there is a slight suppression of the superconductivity induced into the N film by the current injected into it.

In contrast, the deviation of $I_s(\varphi_g)$ from the sinusoidal shape turns out to be significant (see Figure 8a). It can be seen that the critical current I_c achieved at $\varphi_g = \varphi_m > \pi/2$, and that the parameters I_c and φ_m are both dependent on L_I and γ_{BM}.

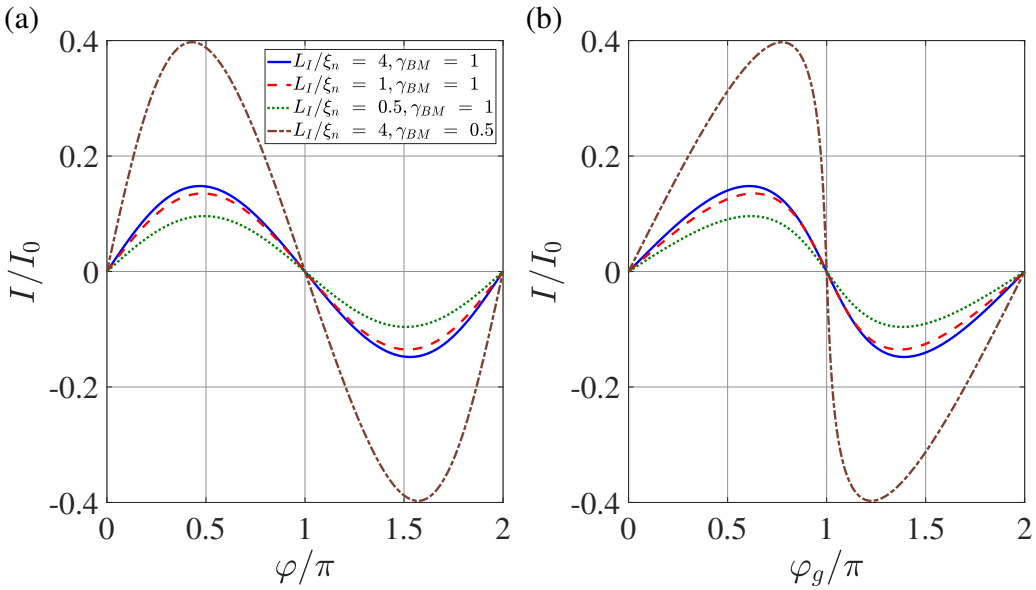

Figure 8. Current–phase relation $I(\varphi)$ (**a**) and dependence of current on the global phase $I(\varphi_g)$ (**b**) calculated for four combinations of L_I and γ_{BM}. These combinations are $(L_I/\xi_n = 4, \gamma_{BM} = 1)$, $(L_I/\xi_n = 1, \gamma_{BM} = 1)$, $(L_I/\xi_n = 0.5, \gamma_{BM} = 1)$, and $(L_I/\xi_n = 4, \gamma_{BM} = 0.5)$. Other parameters are $T/T_c = 0.5$, $d_n/\xi_n = 0.1$, $d_s/\xi_n = 10$, $L = 20$, $\rho_s/\rho_n = 10$, $L_b/\xi_n = 0.1$.

Figure 9 shows the dependence of the critical current I_c and the global critical phase φ_m on the overlap length L_I calculated for different values of the suppression parameters γ_{BM}. The points on the curves in Figure 9b indicate positions in the N film that are spaced from $x = L_b$ by the characteristic length ξ_{eff} (3) calculated for $\omega = \pi T$.

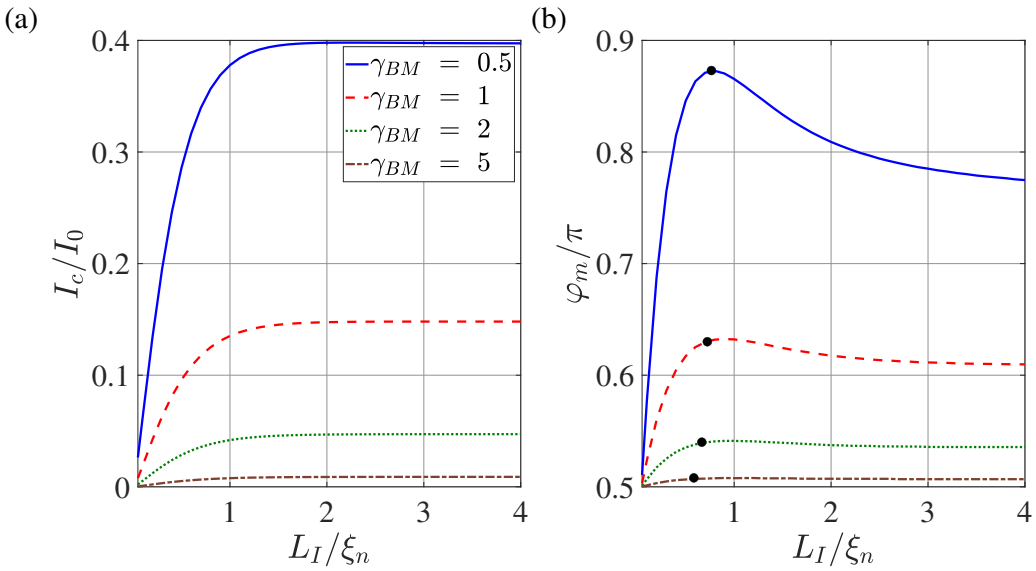

Figure 9. Dependence of the critical current (**a**) and the corresponding global phase (**b**) on the overlap length L_I calculated for $\gamma_{BM} = 0.5, 1, 2, 5$. Other parameters: $T/T_c = 0.5$, $d_n/\xi_n = 0.1$, $d_s/\xi_n = 10$, $L = 20$, $\rho_s/\rho_n = 10$, $L_b/\xi_n = 0.1$. The black dots on the curves indicate the values of functions obtained at a distance removed from $x = L_b/2$ by an amount equal to the effective coherence length ξ_{eff} at $\omega = \pi T$.

It can be seen that with $L_I/\xi_n \gtrsim 2$ both of these parameters are weakly dependent on L_I. With such a noticeable overlap of the S and N films, part of the current has the ability to flow through the N film for a sufficiently long distance before leaking into the S electrode in a vicinity of $x \lesssim L_b/2 + L_I$. This decreases the current concentration in the S film in

the vicinity of $x \gtrsim L_b/2$. At $L_I/\xi \approx 2$, these two areas of current leakage overlap. With a further decrease in L_I, the current concentration region in the S-electrode is compressed and the additional contribution to linear inductance increases. This leads to an increase in φ_m. At $L_I \lesssim \xi_n$, the mechanisms of suppression of superconductivity by current injected into the N region are most pronounced. This is accompanied by a decrease in the critical current; consequently, φ_m.

Figure 10 shows the dependencies of the critical current and φ_m on the suppression parameter γ_{BM} for various overlap lengths L_I. In full accordance with the results presented in Figure 9, it can be seen that with the growth of L_I the dependencies of $Ic(\gamma_{BM})$ and $\varphi_m(\gamma_{BM})$ appear out on the universal curves, demonstrating the independence of these parameters from L_I.

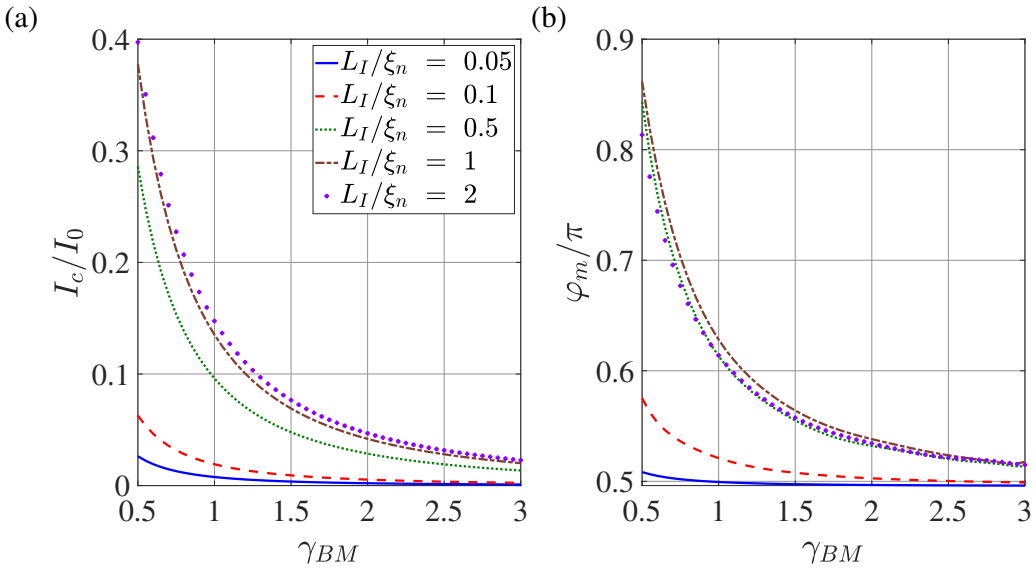

Figure 10. Dependence of the critical current (**a**) and the corresponding global phase (**b**) on the suppression parameter γ_{BM} calculated for $L_I/\xi_n = 0.05, 0.1, 0.5, 1, 2$. Other parameters: $T/T_c = 0.5$, $d_n/\xi_n = 0.1$, $d_s/\xi_n = 10$, $L = 20$, $\rho_s/\rho_n = 10$, $L_b/\xi_n = 0.1$.

7. Discusion

The performed study of electronic transport in planar Josephson SN-N-NS devices clearly demonstrates that the spatial redistribution of the supercurrent in the electrodes results in delocalization of their weak link region and a significant change in the shape of current–phase relation in these structures.

Our predictions can be verified experimentally by direct measurements of the current–phase relationship of these structures as well as by experimental study of the predicted dependence $I_c(L_I)$ shown in Figure 9.

We have shown that as the length of the L_I of the SN interface decreases, the weakest place in the weak link region moves from the N metal to the SN boundaries. In fact, as shown in Figure 9, for values of L_I greater than ξ_{eff}, the critical current of the structure does not depend on L_I. As L_I decreases, the current density injected into the S electrode not only increases, it becomes more spatially homogeneous, meaning that I_c becomes directly proportional to L_I. It is important to note that the degree of symmetry of such a double-barrier structure is determined by the difference in the length of the SN boundaries, and not by the difference in their transparency coefficients.

In the experimental study of structures in which a topological insulator plays the role of a normal metal, this remark is particularly important. The decay length in ballistic channels carrying superconducting current in topological materials can significantly exceed the ξ_n of dirty films of normal metals. Because of this, the $L_I \approx \xi_{eff}$ ratio can be easily realised in a real experimental situation ($L_I \gtrsim 100$ nm). In this case, the subject of experimental research is not the transport properties of a topological insulator; rather, it is the properties of its

least-extended boundary with a superconducting electrode. As the transparency of the SN boundary is not much different from unity, the temperature dependence of the critical current of such a structure does not differ markedly from that predicted for pure ballistic contacts. Therefore, the fact that the experimental dependence $I_c(T)$ coincides with the theoretical dependence for purely ballistic contacts does not provide a clear indication as to which of the structures (SNS or SINIS) was actually studied. Thus, in [45], the presence of two critical currents was detected in the structures obtained by sputtering of Nb on top of Fe-doped $BiSbTe_2Se$ flake. According to the authors, the existence of the second critical current results from the intrinsic superconductivity of the Nb–Fe-doped $BiSbTe_2Se$ interface. On the basis of the conclusions obtained from this work, the fact of the existence of two critical currents can be interpreted in a different way. If the Nb–Fe-doped $BiSbTe_2Se$–Nb contact is not an SNS but an asymmetric SINIS structure, then its critical current is determined by the least extended SN boundary, and the second critical current (a voltage jump on the I-V curve at a finite value of a bias current) occurs as a result of the transition to the normal state of the second-most extended SN interface. From our point of view, the experimental determination of the dependence $I_c(L_I)$ should be an important first step in the study of the parameters of SN-N-NS structures, as it permits experimental evaluation of such important parameters as ξ_{ef} as well as understanding the type of Josephson contact (SNS or SINIS) realized by the geometry of the SN-N-NS contact selected for subsequent experimental studies.

It should be noted that the predicted deformation of the shape of current–phase relationship should be present in the SN-N-NS contacts studied here as well as in any Josephson structure where there is a concentration or other redistribution of the superconducting current in the regions of the S electrodes bordering the weak coupling region, for example, in Dayem and variable thickness bridges.

In Dayem bridges, the effective cross-section of the area where the current is concentrated in the S electrodes decreases due to the narrowing of the width of this area [83]. In variable thickness bridges, the current is concentrated in both the thickness and width of the S electrodes. As in the case of SN-N-NS bridges, the current concentration in DB and BVT structures should be accompanied by an increase in the local values of the inductance of the electrodes per unit of their length, i.e., their significant deviation from the linear inductance of S films away from the constriction. As a consequence, this should lead to the experimental shape of the current phase relation of SN-N-NS, BVT, and DB structures determined using both rf and dc SQUIDs providing $I(\varphi_g)$ and not $I(\varphi)$. The fact that the CPR experimentally obtained in Dayem bridges [15,23,24,27,29,35,84,85] has a shape that coincides with that shown in Figure 8 indirectly confirms the correctness of our results. We emphasise again that in addition to containing information about the contacts themselves, the current phase dependencies obtained experimentally in these works depend on the structure of the current redistribution in their electrodes.

8. Conclusions

The approach we have demonstrated in this paper allows calculation of the parameters of the equivalent scheme of SN-N-NS, BVT, and DB structures. Their representation in the form of a serial connection of the Josephson contact having $I(\varphi_g)$ and the linear inductance of conductive electrodes is useful for the interpretation of experimental data in bridges [13,86], analysis of processes in nano-SQUIDs [1–11],experimental determination of inductance in various low-current superconducting devices [3,9], and in the design of digital circuits [12–14].

The data presented in Figures 8–10 allow us to conclude that the conclusions formulated in [47] about the prospects of using SN-N-NS contacts as control elements of superconducting digital devices are correct if the following conditions are met: the overlapping area of S and N films L_I should exceed $2\xi_n$; and the suppression parameter γ_{BM} should be of the order of one. In this case, the characteristic size of the contact L_g is approximately equal to $L_b + 4\xi_n$, and the shape of the dependence $I(\varphi_g)$ does not differ much from the

sinusoidal one. It is important to note that the numerical results presented in this paper should only be considered as orders of magnitude estimates. Exact values can be obtained by generalising the model to a 3D case, which will be the subject of future work.

Our calculations focused on structures with electrodes made of conventional superconducting materials, where the dirty limit conditions are usually met and the isotropic potential of superconducting electron pairing occurs. In contrast, high-temperature superconducting materials are pure metals; their pairing potential is anisotropic, and has a d-wave or p-wave type symmetry.

This difference is significantly manifested at the boundaries of materials with weak coupling regions, leading to the possible generation of subdominant order parameters and spontaneous currents [87–92]. However, these effects should mainly affect the magnitude of the critical current of the structures. The concentration of the current in the electrode region bordering on the concentrating current weak link occurs independently of the differences formulated above. This means that delocalisation of the weak coupling region and the associated changes in the shape of the current–phase relationship are universal phenomena which should take place regardless of whether conventional or high-temperature superconductors are used as electrodes. Finally, it is important to note that there are geometries that result in current being concentrated in the electrodes at boundary surfaces with weak coupling.

Author Contributions: Formulation of the model, S.B. and M.K.; calculations, V.R. and S.B.; Data curation, N.K. and I.S.; Formal analysis, I.S. and A.G.; Funding acquisition, M.K. and V.S.; writing—original draft preparation, V.R., S.B. and M.K.; writing—review and editing, I.S., V.S. and A.G. All authors have read and agreed to the published version of the manuscript.

Funding: The investigation of the spatial distribution of the order parameter and current–phase dependence was carried out with the financial support of the Strategic Academic Leadership Programme "Priority-2030" (NUST MISIS Grant No. K2-2022-029). The development of the concept of a nanoscale Josephson contact based on a variable thickness bridge (Sections 2–4) was supported by the Russian Science Foundation, Grant No. 20-12-00130 https://rscf.ru/project/20-12-00130/ (accessed on 15 May 2023). The analysis of the electrode influence on the features of current transport was carried out with the help of the Russian Science Foundation, Grant No. 23-72-30004 https://rscf.ru/project/23-72-30004/ (accessed on 15 April 2023). The work of VSS was supported by the Ministry of Science and Higher Education of the Russian Federation (No. FSMG-2023-0014).

Data Availability Statement: The data presented in this study are available on request from the corresponding author.

Acknowledgments: The authors are grateful to V. Boosboom and O.V. Skryabina for useful discussions of the obtained results.

Conflicts of Interest: The authors declare no conflict of interest.

References

1. Hao, L.; Macfarlane, J.C.; Gallop, J.C.; Romans, E.; Cox, D.; Hutson, D.; Chen, J. Spatial Resolution Assessment of Nano-SQUIDs Made by Focused Ion Beam. *IEEE Trans. Appl. Supercond.* **2007**, *17*, 742–745. [CrossRef]
2. Vijay, R.; Levenson-Falk, E.M.; Slichter, D.H.; Siddiqi, I. Approaching ideal weak link behavior with three dimensional aluminum nanobridges. *Appl. Phys. Lett.* **2010**, *96*, 223112. [CrossRef]
3. Wang, H.; Yang, R.; Li, G.; Wu, L.; Liu, X.; Chen, L.; Ren, J.; Wang, Z. Inductance analysis of superconducting quantum interference devices with 3D nano-bridge junctions. *Supercond. Sci. Technol.* **2018**, *31*, 055015. [CrossRef]
4. Russo, R.; Esposito, E.; Crescitelli, A.; Gennaro, E.D.; Granata, C.; Vettoliere, A.; Cristiano, R.; Lisitskiy, M. NanoSQUIDs based on niobium nitride films. *Supercond. Sci. Technol.* **2016**, *30*, 024009. [CrossRef]
5. Holzman, I.; Ivry, Y. On-chip integrable planar NbN nanoSQUID with broad temperature and magnetic-field operation range. *AIP Adv.* **2019**, *9*, 105028. [CrossRef]
6. Shishkin, A.G.; Skryabina, O.V.; Gurtovoi, V.L.; Dizhur, S.E.; Faley, M.I.; Golubov, A.A.; Stolyarov, V.S. Planar MoRe-based direct current nanoSQUID. *Supercond. Sci. Technol.* **2020**, *33*, 065005. [CrossRef]
7. Polychroniou, E.; Gallop, J.; Godfrey, T.; Cox, D.; Long, G.; Chen, J.; Romans, E.; Hao, L. Investigation of NanoSQUIDs Fabricated with a Range of Focused Ion Beam Sources. In *Proceedings of the Journal of Physics: Conference Series*; IOP Publishing: Bristol, UK, 2020; Volume 1559, p. 012015.

8. Faley, M.I.; Liu, Y.; Dunin-Borkowski, R.E. Titanium nitride as a new prospective material for NanoSQUIDs and superconducting nanobridge electronics. *Nanomaterials* **2021**, *11*, 466. [CrossRef] [PubMed]
9. Faley, M.; Fiadziushkin, H.; Frohn, B.; Schüffelgen, P.; Dunin-Borkowski, R. TiN nanobridge Josephson junctions and nanoSQUIDs on SiN-buffered Si. *Supercond. Sci. Technol.* **2022**, *35*, 065001. [CrossRef]
10. Faley, M.I.; Dunin-Borkowski, R.E. A Self-Flux-Biased NanoSQUID with Four NbN-TiN-NbN Nanobridge Josephson Junctions. *Electronics* **2022**, *11*, 1704. [CrossRef]
11. Meti, L.; Long, G.; Godfrey, T.; Potter, J.; Cox, D.; Chapman, G.; Gallop, J.; Romans, E.; Hao, L. Development of flux-tuneable inductive nanobridge SQUIDs for quantum technology applications. *IEEE Trans. Appl. Supercond.* **2023**, *33*, 1–5. [CrossRef]
12. Shelly, C.D.; See, P.; Ireland, J.; Romans, E.J.; Williams, J.M. Weak link nanobridges as single flux quantum elements. *Supercond. Sci. Technol.* **2017**, *30*, 095013. [CrossRef]
13. Collins, J.A.; Rose, C.S.; Casaburi, A. Superconducting Nb Nanobridges for Reduced Footprint and Efficient Next-Generation Electronics. *IEEE Trans. Appl. Supercond.* **2022**, *33*, 1–8. [CrossRef]
14. Thompson, M.L.; Castellanos-Beltran, M.; Hopkins, P.F.; Dresselhaus, P.D.; Benz, S.P. Effects of Nonsinusoidal Current Phase Relationships on Single Flux Quantum Circuits. *IEEE Trans. Appl. Supercond.* **2023**, *33*, 1–5. [CrossRef]
15. Troeman, A.; Van Der Ploeg, S.; Il'Ichev, E.; Meyer, H.G.; Golubov, A.A.; Kupriyanov, M.Y.; Hilgenkamp, H. Temperature dependence measurements of the supercurrent-phase relationship in niobium nanobridges. *Phys. Rev. B* **2008**, *77*, 024509. [CrossRef]
16. Keijers, W.; Baumans, X.D.; Panghotra, R.; Lombardo, J.; Zharinov, V.S.; Kramer, R.B.; Silhanek, A.V.; Van de Vondel, J. Nano-SQUIDs with controllable weak links created via current-induced atom migration. *Nanoscale* **2018**, *10*, 21475–21482. [CrossRef] [PubMed]
17. Montemurro, D.; Golubev, D.S.; Kubatkin, S.; Tafuri, F.; Bauch, T.; Lombardi, F. Enhanced Josephson coupling in hybrid nanojunctions. *Phys. Rev. B* **2023**, *107*, 094517. [CrossRef]
18. Roditchev, D.; Brun, C.; Serrier-Garcia, L.; Cuevas, J.C.; Bessa, V.H.L.; Milošević, M.V.; Debontridder, F.; Stolyarov, V.; Cren, T. Direct observation of Josephson vortex cores. *Nat. Phys.* **2015**, *11*, 332–337. [CrossRef]
19. Jung, M.; Noh, H.; Doh, Y.J.; Song, W.; Chong, Y.; Choi, M.S.; Yoo, Y.; Seo, K.; Kim, N.; Woo, B.C.; et al. Superconducting junction of a single-crystalline Au nanowire for an ideal Josephson device. *ACS Nano* **2011**, *5*, 2271–2276. [CrossRef]
20. Skryabina, O.; Bakurskiy, S.; Shishkin, A.; Klimenko, A.; Napolskii, K.; Klenov, N.; Soloviev, I.; Ryazanov, V.; Golubov, A.; Roditchev, D.; et al. Environment-induced overheating phenomena in Au-nanowire based Josephson junctions. *Sci. Rep.* **2021**, *11*, 15274. [CrossRef]
21. Sotnichuk, S.V.; Skryabina, O.V.; Shishkin, A.G.; Bakurskiy, S.V.; Kupriyanov, M.Y.; Stolyarov, V.S.; Napolskii, K.S. Long Single Au Nanowires in Nb/Au/Nb Josephson Junctions: Implications for Superconducting Microelectronics. *ACS Appl. Nano Mater.* **2022**, *5*, 17059–17066. [CrossRef]
22. Skryabina, O.; Egorov, S.; Goncharova, A.; Klimenko, A.; Kozlov, S.; Ryazanov, V.; Bakurskiy, S.; Kupriyanov, M.Y.; Golubov, A.; Napolskii, K.; et al. Josephson coupling across a long single-crystalline Cu nanowire. *Appl. Phys. Lett.* **2017**, *110*, 222605. [CrossRef]
23. Spanton, E.M.; Deng, M.; Vaitiekėnas, S.; Krogstrup, P.; Nygård, J.; Marcus, C.M.; Moler, K.A. Current–phase relations of few-mode InAs nanowire Josephson junctions. *Nat. Phys.* **2017**, *13*, 1177–1181. [CrossRef]
24. Hart, S.; Cui, Z.; Ménard, G.; Deng, M.; Antipov, A.E.; Lutchyn, R.M.; Krogstrup, P.; Marcus, C.M.; Moler, K.A. Current-phase relations of InAs nanowire Josephson junctions: From interacting to multimode regimes. *Phys. Rev. B* **2019**, *100*, 064523. [CrossRef]
25. Williams, J.; Bestwick, A.; Gallagher, P.; Hong, S.S.; Cui, Y.; Bleich, A.S.; Analytis, J.; Fisher, I.; Goldhaber-Gordon, D. Unconventional Josephson effect in hybrid superconductor-topological insulator devices. *Phys. Rev. Lett.* **2012**, *109*, 056803. [CrossRef]
26. Cho, S.; Dellabetta, B.; Yang, A.; Schneeloch, J.; Xu, Z.; Valla, T.; Gu, G.; Gilbert, M.J.; Mason, N. Symmetry protected Josephson supercurrents in three-dimensional topological insulators. *Nat. Commun.* **2013**, *4*, 1689. [CrossRef] [PubMed]
27. Sochnikov, I.; Bestwick, A.J.; Williams, J.R.; Lippman, T.M.; Fisher, I.R.; Goldhaber-Gordon, D.; Kirtley, J.R.; Moler, K.A. Direct measurement of current-phase relations in superconductor/topological insulator/superconductor junctions. *Nano Lett.* **2013**, *13*, 3086–3092. [CrossRef] [PubMed]
28. Galletti, L.; Charpentier, S.; Iavarone, M.; Lucignano, P.; Massarotti, D.; Arpaia, R.; Suzuki, Y.; Kadowaki, K.; Bauch, T.; Tagliacozzo, A.; et al. Influence of topological edge states on the properties of Al/Bi 2 Se 3/Al hybrid Josephson devices. *Phys. Rev. B* **2014**, *89*, 134512. [CrossRef]
29. Sochnikov, I.; Maier, L.; Watson, C.A.; Kirtley, J.R.; Gould, C.; Tkachov, G.; Hankiewicz, E.M.; Brüne, C.; Buhmann, H.; Molenkamp, L.W.; et al. Nonsinusoidal current-phase relationship in Josephson junctions from the 3D topological insulator HgTe. *Phys. Rev. Lett.* **2015**, *114*, 066801. [CrossRef]
30. Kurter, C.; Finck, A.D.; Hor, Y.S.; Van Harlingen, D.J. Evidence for an anomalous current–phase relation in topological insulator Josephson junctions. *Nat. Commun.* **2015**, *6*, 7130. [CrossRef]
31. Wiedenmann, J.; Bocquillon, E.; Deacon, R.S.; Hartinger, S.; Herrmann, O.; Klapwijk, T.M.; Maier, L.; Ames, C.; Brüne, C.; Gould, C.; et al. 4 π-periodic Josephson supercurrent in HgTe-based topological Josephson junctions. *Nat. Commun.* **2016**, *7*, 10303. [CrossRef]

32. Bocquillon, E.; Deacon, R.S.; Wiedenmann, J.; Leubner, P.; Klapwijk, T.M.; Brüne, C.; Ishibashi, K.; Buhmann, H.; Molenkamp, L.W. Gapless Andreev bound states in the quantum spin Hall insulator HgTe. *Nat. Nanotechnol.* **2017**, *12*, 137–143. [CrossRef] [PubMed]
33. Dufouleur, J.; Veyrat, L.; Dassonneville, B.; Xypakis, E.; Bardarson, J.H.; Nowka, C.; Hampel, S.; Schumann, J.; Eichler, B.; Schmidt, O.; et al. Weakly-coupled quasi-1D helical modes in disordered 3D topological insulator quantum wires. *Sci. Rep.* **2017**, *7*, 45276. [CrossRef]
34. Li, C.; De Ronde, B.; De Boer, J.; Ridderbos, J.; Zwanenburg, F.; Huang, Y.; Golubov, A.; Brinkman, A. Zeeman-effect-induced 0- π transitions in ballistic Dirac semimetal Josephson junctions. *Phys. Rev. Lett.* **2019**, *123*, 026802. [CrossRef] [PubMed]
35. Kayyalha, M.; Kargarian, M.; Kazakov, A.; Miotkowski, I.; Galitski, V.M.; Yakovenko, V.M.; Rokhinson, L.P.; Chen, Y.P. Anomalous low-temperature enhancement of supercurrent in topological-insulator nanoribbon Josephson junctions: Evidence for low-energy Andreev bound states. *Phys. Rev. Lett.* **2019**, *122*, 047003. [CrossRef] [PubMed]
36. Kunakova, G.; Bauch, T.; Trabaldo, E.; Andzane, J.; Erts, D.; Lombardi, F. High transparency Bi2Se3 topological insulator nanoribbon Josephson junctions with low resistive noise properties. *Appl. Phys. Lett.* **2019**, *115*, 172601. [CrossRef]
37. Kunakova, G.; Surendran, A.P.; Montemurro, D.; Salvato, M.; Golubev, D.; Andzane, J.; Erts, D.; Bauch, T.; Lombardi, F. Topological insulator nanoribbon Josephson junctions: Evidence for size effects in transport properties. *J. Appl. Phys.* **2020**, *128*, 194304. [CrossRef]
38. Stolyarov, V.S.; Yakovlev, D.S.; Kozlov, S.N.; Skryabina, O.V.; Lvov, D.S.; Gumarov, A.I.; Emelyanova, O.V.; Dzhumaev, P.S.; Shchetinin, I.V.; Hovhannisyan, R.A.; et al. Josephson current mediated by ballistic topological states in Bi_2Te_2. $3Se_{0.7}$ single nanocrystals. *Commun. Mater.* **2020**, *1*, 38. [CrossRef]
39. Kim, N.H.; Kim, H.S.; Hou, Y.; Yu, D.; Doh, Y.J. Superconducting quantum interference devices made of Sb-doped Bi2Se3 topological insulator nanoribbons. *Curr. Appl. Phys.* **2020**, *20*, 680–685. [CrossRef]
40. Kayyalha, M.; Kazakov, A.; Miotkowski, I.; Khlebnikov, S.; Rokhinson, L.P.; Chen, Y.P. Highly skewed current–phase relation in superconductor–topological insulator–superconductor Josephson junctions. *NPJ Quantum Mater.* **2020**, *5*, 7. [CrossRef]
41. Zhang, J.; Jalil, A.R.; Tse, P.L.; Kölzer, J.; Rosenbach, D.; Valencia, H.; Luysberg, M.; Mikulics, M.; Panaitov, G.; Grützmacher, D.; et al. Proximity-Effect-Induced Superconductivity in Nb/Sb2Te3-Nanoribbon/Nb Junctions. *Ann. Der Phys.* **2020**, *532*, 2000273. [CrossRef]
42. Tse, P.L.; Tian, F.; Mugica-Sanchez, L.; Ruger, O.; Undisz, A.; Möthrath, G.; Ronning, C.; Takahashi, S.; Lu, J.G. Microwave AC Resonance Induced Phase Change in Sb2Te3 Nanowires. *Nano Lett.* **2020**, *20*, 8668–8674. [CrossRef] [PubMed]
43. Stolyarov, V.S.; Pons, S.; Vlaic, S.; Remizov, S.V.; Shapiro, D.S.; Brun, C.; Bozhko, S.I.; Cren, T.; Menshchikova, T.V.; Chulkov, E.V.; et al. Superconducting long-range proximity effect through the atomically flat interface of a Bi_2Te_3 topological insulator. *J. Phys. Chem. Lett.* **2021**, *12*, 9068–9075. [CrossRef] [PubMed]
44. Stolyarov, V.S.; Roditchev, D.; Gurtovoi, V.L.; Kozlov, S.N.; Yakovlev, D.S.; Skryabina, O.V.; Vinokur, V.M.; Golubov, A.A. Resonant Oscillations of Josephson Current in Nb-$Bi_2Te_{2.3}Se_{0.7}$-Nb Junctions. *Adv. Quantum Technol.* **2022**, *5*, 2100124. [CrossRef]
45. Kudriashov, A.; Babich, I.; Hovhannisyan, R.A.; Shishkin, A.G.; Kozlov, S.N.; Fedorov, A.; Vyalikh, D.V.; Khestanova, E.; Kupriyanov, M.Y.; Stolyarov, V.S. Revealing Intrinsic Superconductivity of the Nb/$BiSbTe_2Se$ Interface. *Adv. Funct. Mater.* **2022**, *32*, 2209853. [CrossRef]
46. Surendran, P.A.; Montemurro, D.; Kunakova, G.; Palermo, X.; Niherysh, K.; Trabaldo, E.; Golubev, D.; Andzane, J.; Erts, D.; Lombardi, F.; et al. Current-phase relation of a short multi-mode Bi2Se3 topological insulator nanoribbon Josephson junction with ballistic transport modes. *Supercond. Sci. Technol.* **2023**, *36*, 064003. [CrossRef]
47. Soloviev, I.; Bakurskiy, S.; Ruzhickiy, V.; Klenov, N.; Kupriyanov, M.; Golubov, A.; Skryabina, O.; Stolyarov, V. Miniaturization of Josephson Junctions for Digital Superconducting Circuits. *Phys. Rev. Appl.* **2021**, *16*, 044060. [CrossRef]
48. Marychev, P.M.; Vodolazov, D.Y. A Josephson junction based on a highly disordered superconductor/low-resistivity normal metal bilayer. *Beilstein J. Nanotechnol.* **2020**, *11*, 858–865. [CrossRef]
49. Bosboom, V.; der Vegt, J.J.W.V.; Kupriyanov, M.Y.; Golubov, A.A. Selfconsistent 3D model of SN-N-NS Josephson junctions. *Supercond. Sci. Technol.* **2021**, *34*, 115022. [CrossRef]
50. Cuthbert, M.; DeBenedictis, E.; Fagaly, R.L.; Fagas, G.; Febvre, P.; Fourie, C.; Frank, M.; Gupta, D.; Herr, A.; Holmes, D.S.; et al. International roadmap for devices and systems. In *Cryogenic Electronics and Quantum Information Processing*; IEEE: Piscataway, NJ, USA, 2022.
51. Likharev, K.K. Superconducting weak links. *Rev. Mod. Phys.* **1979**, *51*, 101–159. [CrossRef]
52. Golubov, A.A.; Kupriyanov, M.Y.; Il'ichev, E. The current-phase relation in Josephson junctions. *Rev. Mod. Phys.* **2004**, *76*, 411–469. [CrossRef]
53. Likharev, K.K. Vortex motion and the Josephson effect in superconducting thin bridges. *Zh. Eksp. Teor. Fiz.* **1971**, *61*, 1700–1711.
54. Kulik, I.O.; Omel'yanchuk, A.N. Contribution to the microscopic theory of the Josephson effect in superconducting bridges. *Pis'ma Zh. Eksp. Teor. Fiz.* **1975**, *21*, 216–219.
55. Likharev, K.K.; Yakobson, L.A. Dynamical properties of superconducting filaments of finite length. *Zh. Eksp. Teor. Fiz.* **1975**, *68*, 1150–1160.
56. Likharev, K.K. The relation $J_s(\varphi)$ for SNS bridges of variable thickness. *Pis'ma Zh. Tekh. Fiz.* **1976**, *2*, 29.
57. Kupriyanov, M.Y.; Likharev, K.K.; Lukichev, V.F. Influence of effective electron interaction on the critical current of Josephson weak links. *Zh. Eksp. Teor. Fiz.* **1982**, *83*, 431–441. [CrossRef]

58. Dubos, P.; Courtois, H.; Pannetier, B.; Wilhelm, F.K.; Zaikin, A.D.; Schön, G. Josephson critical current in a long mesoscopic S-N-S junction. *Phys. Rev. B* **2001**, *63*, 064502. [CrossRef]
59. Ivanov, Z.G.; Kupriyanov, M.Y.; Likharev, K.K.; Meriakri, S.V.; Snigirev, O.V. Boundary-conditions for the Usadel and Eilenberger equations, and properties of dirty SNS sandwich-type junctions. *Sov. J. Low. Temp. Phys.* **1981**, *7*, 274–281.
60. Kupriyanov, M.Y.; Lukichev, V.F. The influence of proximity effect in electrodes on the stationary properties of S-N-S Josephson structures. *Sov. J. Low. Temp. Phys.* **1982**, *8*, 526–529.
61. Zubkov, A.; Kupriyanov, M. Effect of depairing in electrodes on the stationary properties of weak links. *Sov. J. Low Temp. Phys.* **1983**, *5*, 279–281.
62. Barash, Y.S. Anharmonic Josephson current in junctions with an interface pair breaking. *Phys. Rev. B* **2012**, *85*, 100503. [CrossRef]
63. Kupriyanov, M. Effect of a finite transmission of the insulating layer on the properties of SIS tunnel-junctions. *JETP Lett.* **1992**, *56*, 399–405.
64. Golubov, A.; Kupriyanov, M. The current phase relation in Josephson tunnel junctions. *JETP Lett.* **2015**, *81*, 335–341. [CrossRef]
65. Osin, A.S.; Fominov, Y.V. Superconducting phases and the second Josephson harmonic in tunnel junctions between diffusive superconductors. *Phys. Rev. B* **2021**, *104*, 064514. [CrossRef]
66. Osin, A.S.; Fominov, Y.V. Comment on "Josephson Current as a Boundary Condition for Gor'kov Equations. *J. Supercond. Nov. Magn.* **2022**, *36*, 55–58. [CrossRef]
67. Semenov, V.K.; Polyakov, Y.A.; Tolpygo, S.K. Very Large Scale Integration of Josephson-Junction-Based Superconductor Random Access Memories. *IEEE Trans. Appl. Supercond.* **2019**, *29*, 1302809. [CrossRef]
68. Kuprianov, M.Y.; Lukichev, V.F. Effect of boundary transparency on critical current in dirty SS'S structures. *Zh. Eksp. Teor. Fiz.* **1988**, *94*, 139–149.
69. Golubov, A.A.; Kuprianov, M.Y. Josephson effect in SNlNS and SNIS tunnel structures with finite transparency of the SN boundaries. *Zh. Eksp. Teor. Fiz.* **1989**, *96*, 1420–1433.
70. Golubov, A.A.; Houwman, E.P.; Gijsbertsen, J.G.; Krasnov, V.M.; Flokstra, J.; Rogalla, H.; Kupriyanov, M.Y. Proximity effect in superconductor-insulator-superconductor Josephson tunnel junctions: Theory and experiment. *Phys. Rev. B* **1995**, *51*, 1073–1089. [CrossRef] [PubMed]
71. Zehnder, A.; Lerch, P.; Zhao, S.P.; Nussbaumer, T.; Kirk, E.C.; Ott, H.R. Proximity effects in Nb/Al-AlO$_x$-Al/Nb superconducting tunneling junctions. *Phys. Rev. B* **1999**, *59*, 8875. [CrossRef]
72. Brammertz, G.; Poelaert, A.; Golubov, A.A.; Verhoeve, P.; Peacock, A.; Rogalla, H. Generalized proximity effect model in superconducting bi- and trilayer films. *J. Appl. Phys.* **2001**, *90*, 355–364. [CrossRef]
73. Baxter, D.V.; Steenwyk, S.D.; Bass, J.; Pratt, W.P. Resistance and spin-direction memory loss at Nb/Cu interfaces. *J. Appl. Phys.* **1999**, *85*, 4545. [CrossRef]
74. Park, W.; Baxter, D.V.; Steenwyk, S.; Moraru, I.; Pratt, W.P.; Bass, J. Measurement of resistance and spin-memory loss (spin relaxation) at interfaces using sputtered current perpendicular-to-plane exchange-biased spin valves. *Phys. Rev. B* **2000**, *62*, 1178. [CrossRef]
75. Sharma, A.; Romero, J.A.; Theodoropoulou, N.; Loloee, R.; Pratt, J.W.P.; Bass, J. Specific resistance and scattering asymmetry of Py/Pd, Fe/V, Fe/Nb, and Co/Pt interfaces. *J. Appl. Phys.* **2007**, *102*, 113916. [CrossRef]
76. Tuuli, E.; Gloos, K. Normal reflection at superconductor - normal metal interfaces due to Fermi surface mismatch. *J. Phys. Conf. Ser.* **2012**, *400*, 042066. [CrossRef]
77. Bass, J. CPP magnetoresistance of magnetic multilayers: A critical review. *J. Magn. Magn. Mater.* **2016**, *408*, 244–320. [CrossRef]
78. Stolyarov, V.S.; Tristan, C.; Christophe, B.; Golovchanskiy, I.A.; Skryabina, O.V.; Kasatonov, D.I.; Khapaev, M.M.; Kupriyanov, M.Y.; Golubov, A.A.; Dimitri, R. Expansion of a superconducting vortex core into a diffusive metal. *Nat. Commun.* **2018**, *2*, 2277. [CrossRef]
79. Tolpygo, S.K.; Bolkhovsky, V.; Rastogi, R.; Zarr, S.; Golden, E.; Weir, T.J.; Johnson, L.M.; Semenov, V.K.; Gouker, M.A. A 150-nm process node of an eight-Nb-layer fully planarized process for superconductor electronics. In Proceedings of the Applied Superconductivity Conference, ASC 2020 Virtual Conference. Superconductivity News Forum (SNF), Virtual, 24 October–7 November 2020; Volume 14, p. STP669 Wk1EOr3B-01. Available online: https://snf.ieeecsc.org/issues/snfissue-no-49-march-2021 (accessed on 15 May 2023).
80. Golikova, T.E.; Hubler, F.; Beckmann, D.; Klenov, N.V.; Bakurskiy, S.V.; Kupriyanov, M.Y.; Batov, I.E.; Ryazanov, V.V. Critical current in planar SNS Josephson junctions. *JETP Lett.* **2012**, *96*, 668–673. [CrossRef]
81. Usadel, K.D. Generalized diffusion equation for superconducting alloys. *Phys. Rev. Lett.* **1970**, *25*, 507–509. [CrossRef]
82. Zubkov, A.A.; Kupriyanov, M.Y.; Semyonov, V.K. Steady-state Properties of the Josephson Junction with Direct Conduction. *Fiz. Nizk. Temp.* **1981**, *7*, 1365–1371.
83. Vijay, R.; Sau, J.; Cohen, M.L.; Siddiqi, I. Optimizing anharmonicity in nanoscale weak link Josephson junction oscillators. *Phys. Rev. Lett.* **2009**, *103*, 087003. [CrossRef]
84. Assouline, A.; Feuillet-Palma, C.; Bergeal, N.; Zhang, T.; Mottaghizadeh, A.; Zimmers, A.; Lhuillier, E.; Eddrie, M.; Atkinson, P.; Aprili, M.; et al. Spin-Orbit induced phase-shift in Bi2Se3 Josephson junctions. *Nat. Commun.* **2019**, *10*, 126. [CrossRef] [PubMed]
85. Chen, L.; Wu, L.; Wang, Y.; Pan, Y.; Zhang, D.; Zeng, J.; Liu, X.; Ma, L.; Peng, W.; Wang, Y.; et al. Miniaturization of the Superconducting Memory Cell via a Three-Dimensional Nb Nano-superconducting Quantum Interference Device. *ACS Nano* **2020**, *14*, 11002–11008. [CrossRef] [PubMed]

86. Ruhtinas, A.; Maasilta, I.J. Highly tunable NbTiN Josephson junctions fabricated with focused helium ion beam. *arXiv* **2023**, arXiv:2303.17348.
87. Golubov, A.A.; Kupriyanov, M.Y. Anomalous proximity effect in d-wave superconductors. *JETP Lett.* **1998**, *67*, 501–507. [CrossRef]
88. Golubov, A.A.; Kupriyanov, M.Y. Surface electron scattering in d-wave superconductors. *JETP Lett.* **1999**, *69*, 262–267. [CrossRef]
89. Bakurskiy, S.V.; Golubov, A.A.; Kupriyanov, M.Y.; Yada, K.; Tanaka, Y. Anomalous surface states at interfaces in p -wave superconductors. *Phys. Rev. B* **2014**, *90*, 064513-1–064513-10. [CrossRef]
90. Bakurskiy, S.; Klenov, N.; Soloviev, I.; Kupriyanov, M.Y.; Golubov, A. Observability of surface currents in p-wave superconductors. *Supercond. Sci. Technol.* **2017**, *30*, 044005. [CrossRef]
91. Bakurskiy, S.; Fominov, Y.V.; Shevchun, A.; Asano, Y.; Tanaka, Y.; Kupriyanov, M.Y.; Golubov, A.; Trunin, M.; Kashiwaya, H.; Kashiwaya, S.; et al. Local impedance on a rough surface of a chiral p-wave superconductor. *Phys. Rev. B* **2018**, *98*, 134508. [CrossRef]
92. Suzuki, S.I.; Golubov, A.A. Robustness of chiral surface current and subdominant *s*-wave Cooper pairs. *arXiv* **2023**, arXiv:2305.18018.